Identification and classification of archaeological materials from Bronze age gold mining site Ada Tepe (Bulgaria) using rock magnetism

Neli Jordanova[1*], Diana Jordanova[1], Emilia Tcherkezova[1], Hristo Popov[2], Antonia Mokreva[1], Plamen Georgiev[2], Ruslan Stoychev[3]

1 – National Institute of Geophysics, Geodesy and Geography, Bulgarian Academy of Sciences
2 – National Archaeological Institute with Museum, Bulgarian Academy of Sciences
3 – Institute of Art Studies, Bulgarian Academy of Sciences

* corresponding author e-mail: neli_jordanova@hotmail.com

Abstract

Collection of materials from the most ancient open-pit gold mine in Europe has been investigated using mineral magnetic methods as part of the multi-disciplinary research of the site. The aim of the study was to employ rock-magnetic characteristics (magnetic susceptibility, anhysteretic remanent magnetization, isothermal remanent magnetization and various magnetic grain-size dependent ratios) for classification of a collection of 177 samples, taken from Late Bronze age waste heaps, pristine rocks, natural soils and soils from cultural layers. Factor analysis and k-means cluster analysis revealed that four clusters explain the best mineral magnetic data. Results from the thermomagnetic analysis and thermal demagnetization of composite isothermal remanence proved that the main magnetic minerals in the collection are magnetite, hematite and goethite. Based on the magnetic properties, samples from clusters 1 and 3 were identified as influenced by fire – archaeological structures and waste heaps with the use of fire setting, respectively. Samples belonging to cluster 3 were dominated by goethite and hematite, thus identified as rock residues. Materials grouped in cluster 4 showed magnetic characteristics typical of natural soils and were thus related to this class of materials. The obtained clustering of the samples agreed well with their archaeological assignment. Spatial distribution of cluster members across the site provides valuable environmental information for the location of mining activities, their lateral spread and the technology used. It was concluded that magnetic mineral analysis is a precise, sensitive and highly effective method for characterization and classification of materials from ancient mining.

Keywords: Late Bronze age gold mine; iron oxides; rock magnetism; ancient mining waste heaps, fire setting, anthropogenic soils

1. Introduction

Research on ancient gold mining is mainly focused on the archaeometallurgical investigations aiming at identification of the ore province (i.e. the source of the raw metal) and geochemical characterization of the gold artifacts (e.g. Chapman et al., 2006; Baron et al., 2019). However, full understanding of the sequence ore deposit – mining – processing – gold artifacts production is not possible without detailed knowledge about the ancient mining techniques, process organization and time evolution of the technology utilized. Application of a wide range if interdisciplinary methods could provide clues for discovering relics of ancient mining and ore-processing activities, as well as for reconstructing the methods utilized by the ancient miners and the effects they posed on the environment. One analytical evidence-based approach for obtaining such information is provided by rock-magnetic methods (Evans and Heller, 2003).

Late Bronze Age open-pit gold mine at Ada Tepe in the Easthern Rhodopes (South-Eastern Bulgaria) has been intensively studied during the last decade (Popov and Jockenhövel, 2011; Popov et al., 2017; Jockenhövel and Popov 2018; Popov, 2018 and references therein). The most recent radiocarbon dates obtained suggest that gold mining at the site had started in the early 15th century BC and lasted not more than two centuries (Popov and Jockenhövel, 2018). Based on this and available research on other studied ancient gold mining sites, Ada Tepe is regarded as the oldest known open pit gold mine in Europe at this stage of the development of the mining archaeology. Extensive interdisciplinary research has been carried out on the site (Popov et al., 2014; Popov et al., 2017; Tcherkezova et al., 2014; Tsintsov et al., 2016), in order to elucidate the technological *chaîne opératoire* of the mining activities, but also other aspects, related to settlement organization, cultural and economic contacts, trading, etc.

Comprehensive mineralogical investigations of the major geological strata building up the Ada Tepe hill have shown that the gold mineralization is closely related to iron oxides/hydroxides (Tsintsov et al., 2016). However, detailed mineralogical investigations of heavy mineral extracts (Ajdanlijsky et al., 2008) or single mineral grains (Tsintsov et al., 2016))/veins (Marinova et al., 2014) cannot be performed on large collections of samples.

Contrary to this restriction, mineral magnetic studies of natural rocks/sediments/soils are routinely carried out on numerous samples, giving high-resolution and very precise data about the kind of the iron (hydr)oxides, their grain size and concentration (Thompson and Oldfield, 1986; Evans and Heller, 2003; Jordanova, 2016). In addition, up-to-date measurement facilities (rock magnetometers, magnetic susceptibility bridges, etc.) are able to identify even trace amounts of iron oxides in natural samples with very high precision (Evans and Heller, 2003). Another favorable factor for applying mineral magnetic methods for investigation of this ancient mining site is the evidence existing about the use of fire-setting by the ancient miners (Popov et al., 2014; Popov et al., 2018). Heating generated by firing causes strong thermal transformations in iron (oxy)hydroxides (Cornell and Schwertmann, 2003) with end-products depending on the environmental conditions during thermal treatment (Zboril et al., 2002).

Rock-magnetic investigations, revealing the mineral magnetic context of various materials from Ada Tepe site were carried out in order to probe the appropriateness of this method for elucidation of the usage of archaeological structures as well as identification of the anthropogenic influence across the site. The success of the study relies on the well established high sensitivity of the forms, concentrations and grain sizes of Fe oxides on the environmental conditions (Cornell and Schwertmann, 2003). Moreover, in most surface environments exactly the iron oxides determine the color of the soils, rocks and sediments due to their high pigmenting ability (Barron and Torrent, 1986; Azzali et el., 2011).

2. Site description

Ada Tepe is situated about 3 km south of the town of Krumovgrad in the Eastern Rhodopes, South-Eastern Bulgaria (Fig. 1). The region is part of the Eastern Rhodopes Massif, which hosts the eastern part of a large metamorphic complex (Marchev et al., 2004). The massif is associated with late Cretaceous–Miocene extension, which exposed the underlying lower crust rocks. The host rocks of Ada tepe deposit are the Maastrichtian–Paleocene sedimentary rocks of the Shavarovo Formation. They are represented by metamorphic blocks, breccia, conglomerates, sandstone, marls and argillaceous limestone (Goranov and Atanasov, 1992). The low-sulfidation epithermal gold deposit is represented by: (1) a massive, tabular ore body above the Tokachka detachment fault; and (2) open space filling ores along predominantly east–west oriented listric faults. The gold mineralization is represented mainly by electrum found in micrometer-sized single grains, nests and thin veins.

The electrum is deposited in low-temperature hydrothermally altered rocks (Marinova, 2006). Soils in the area are mainly shallow Chromic Luvisols. According to the CORINE Land Cover nomenclature (CORINE Land Cover, 2018) the vegetation cover in the investigated area is dominated by broad-leaved and mixed forest species.

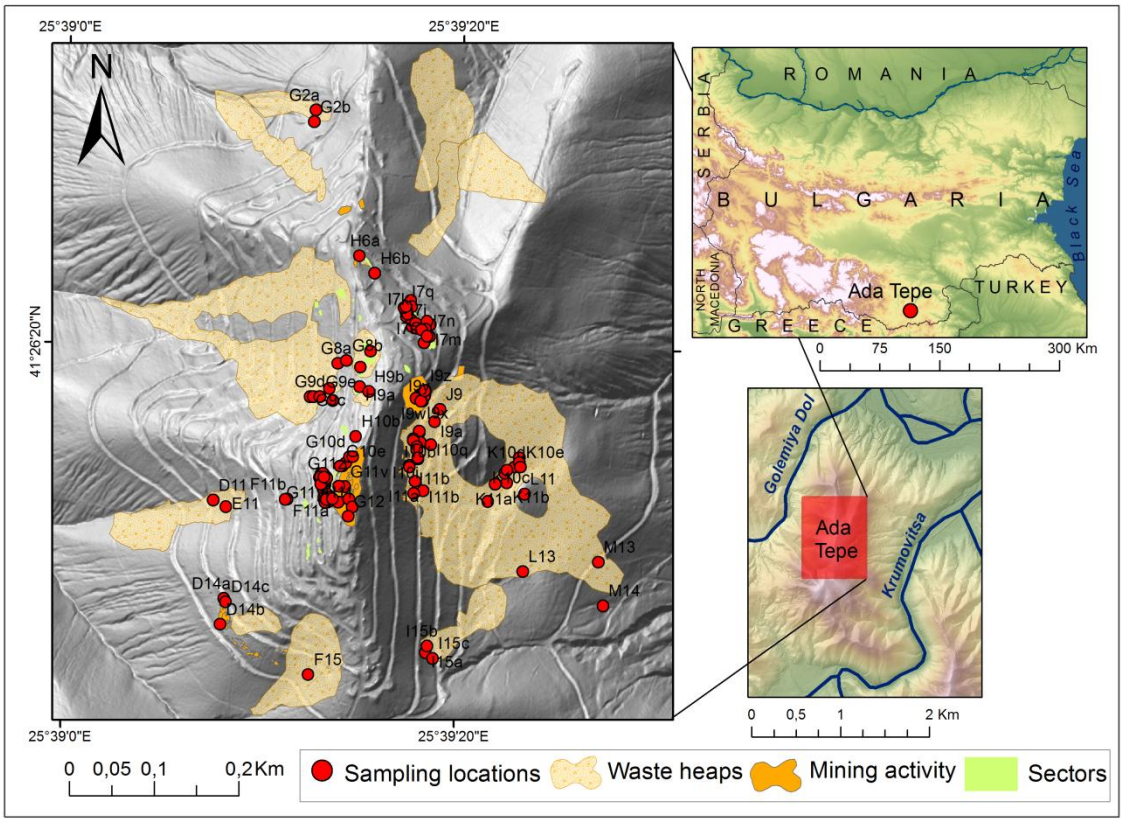

Figure 1*. Site location of the ancient gold mine Ada Tepe at large and regional scale. Detailed map with location of the sampling points, waste heaps, mining areas, and some sectors of archaeological excavations is shown enlarged and denoted in different colors according to the legend (Data sources: samples and sampling locations: E. Tcherkezova, P. Georgiev, R. Stoychev, 2011-2015; geodetic survey: B. Giaourova and Geokom EOOD, Kardzhali; waste heaps mapping: P. Georgiev; hillshade map, calculated on the basis of a precise Digital Terrain Model with grid size 1 m using data from Airborne Laser Scanning (ALS, also known as LiDAR): E. Tcherkezova; ALS scanning and data: Blom EOOD, December 2010). Data source for the terrain of Bulgaria and the neighboring countries: http://www.viewfinderpanoramas.org/Coverage%20map%20viewfinderpanoramas_org3.htm (Accessed: 01/03/2020).*

Archaeological excavations at Ada Tepe began the team of Dr. G. Nehrizov in 2001. During the period 2001-2005 extensive rescue excavations at the summit have been carried

out. Various remains of human activities from different historical epochs spanning the middle of the second millennium B.C. until the late Hellenistic (III-I. c. B.C.) and the late Antique (IV-V. A.D.) have been discovered (Popov and Nikov, 2018; Popov, 2018). The present study is related to the remains of the late Bronze age gold mine (Fig. 1, Fig. 2, Figures S_1-S_4 from Supporting Information), identified and excavated in 2005 and during the period 2008-2015. The gold mine is related to the earliest human presence at the Ada Tepe hill. As mentioned before, according to the numerous radiocarbon dating analyses and evaluation of their stratigraphic and functional context, the ore mining began not later than the beginning of the XVth century B.C. and ended at XIIIth c. B.C. the latest.

Figure 2. Stratigraphic profile of a waste heap from the eastern slope of Ada Tepe.

Remains from the gold mine and its satellite structures are arranged at an area of over 200 000 m^2 on the summit and the elevated parts of the slopes from 340-350 m a.s.l. up to 495 m a.s.l. (the hilltop of Ada Tepe) (Fig. 1). Archaeological structures have various functional character – i) ore production; ii) waste heaps related to primary ore mining and

sorting; iii) heaps related to ore-preparing activities; iv) working stages for ore-processing; v) concomitant settlements (two settlements were discovered - at the North-Eastern slope and at the central part of the summit) and remains from subsidiary buildings, set nearby the technological areas (Supporting Information, Figures S_1-S_5). The data acquired during the studies revealed an ancient open-pit gold mine for mining gold from host rocks (Popov et al., 2018). Archaeological evidence from Ada Tepe ancient mine significantly influenced the chronology of the open-pit gold mining in prehistoric times in Europe and demonstrated a high level of technological development attained by the ancient miners.

An important source of information for the study of the ore mining and processing is the technological waste material of crushed rocks. The waste material from the ancient gold mining was stored by the ancient miners in numerous rock heaps spread at a large area across the hill (Popov et al., 2017). Heap materials exhibited different colors as compared to host rocks (Fig. 2 and Fig. S_5 from Supporting Information). Sediments and hydrothermally altered rocks in the terrains with highest elevation of Ada Tepe usually displayed grey and yellow color, in rare cases yellow-brown color. In contrast, the rock fragments in the waste heaps usually had darker, red to red-brown color which cannot be related to natural geological processes (Popov et al., 2018), but rather to anthropogenic influence and specifically – to the use of fire-setting in order to extract the gold ore (Weisgerber and Willies, 2000). The use of fire-setting in the ancient ore mining is a method which had left distinguishable traces in many mountain-archaeological sites (Craddok 1992; Craddock 1995; Weisgerber and Willies 2000; Domergue 2008 ; Stöllner 2012, etc.), including also Ada Tepe (Popov et al., 2014). An archaeological experiment at Ada Tepe was carried out in 2011, in order to reconstruct various phases of the *chaîne opératoire* during gold mining and ore-preparing activities and to compare materials extracted as a result of the archaeological experiment and the authentic prehistoric materials found during the excavations (Popov et al., 2014). The present rock magnetic study is a step forward in the overall strategy for investigation of the technological activities related to the functioning of Ada Tepe Late Bronze age gold mine. The data acquired are employed for establishing wider inter-disciplinary tools for analysis, topographic and chronological reconstruction of the various units in the technological process.

3. Samples and methods

Loose samples (177 in total) are taken from different archaeological structures (waste heaps, places connected with primary mining activities, ore-preparing working places, mounds, cultural layers and destructions from houses from settlement areas – different areas,

connected with remains of anthropogenic presence on the hilltop of Ada Tepe in general. Sampling is carried out in all major sectors where large-scale archaeological rescue excavations were implemented during the period 2010-2015 (eastern slopes, western slopes, north slopes, ridge, Fig. 1). Sampling sites are listed and described in Supporting Information.

In the laboratory, samples have been prepared for laboratory magnetic measurements. After crushing the material, it was sieved through 2 mm sieve. Loose bulk material filled in 10 cm^3 containers is used for measurements of mass specific magnetic susceptibility (χ) and frequency dependent magnetic susceptibility (χ_{fd}), using kappa bridge MFK2-FA (AGICO Ltd., Czech Republic). Solid cubes with 2 cm side have been prepared by mixing 2 grams of bulk material with small amount of gypsum and water, stirred and left to dry in molds. After drying, the molds were removed and the samples were used for acquisition and measurements of laboratory magnetic remanences. Anhysteretic remanent magnetization (ARM) was induced applying 100mT maximum amplitude of the AF field and superimposed 0.1mT steady dc field using a Molspin AF-demagnetizer with an ARM attachment (Molspin Ltd., UK). Isothermal remanent magnetization (IRM) in 2 Tesla field (IRM_{2T}) was imparted using ASC pulse magnetizer Model IM-10-30 (ASC Scientific, USA). Back-field magnetization at 300mT is subsequently imparted (IRM_{300mT}) for calculation of the S-ratio ($S = -IRM_{300mT}/IRM_{2T}$) (Thompson and Oldfield, 1986). Remanence measurements were carried out using JR-6A automatic spinner magnetometer (AGICO Ltd., Czech Republic). Selected samples were used for stepwise acquisition of IRM in fields up to 5Tesla. Stepwise thermal demagnetization of composite 2-axis IRM up to 700^oC is utilized for identification of the magnetic mineralogy through establishing the unblocking temperature spectra of the magnetically soft fraction of IRM (0-300 mT) and magnetically hard fraction, acquired in the interval (300 mT – 2T) (Lowrie, 1990).. Curie temperature(s) of the magnetic minerals in selected samples were registered using high-temperature behavior of magnetic susceptibility up to 700°C, measured with CS-23 high-temperature furnace, attached to KLY-2 susceptibility bridge (AGICO, Czech Republic).

2. Results

2.1. Mineral magnetic parameters: descriptive statistics

The aim of the magnetic studies carried out is to define a set of magnetic criteria for discriminating samples with different origin and thermal history, thus relevant to various levels of human impact on the environment. The initial examination of the experimental data

consists of basic descriptive statistics, which gives information on the data distributions, mean values and range of variations of the parameters examined (Table 1). The magnetic parameters which are sensitive mainly to the concentration of the strongly magnetic iron oxides in the samples are: magnetic susceptibility (χ), frequency dependent magnetic susceptibility (χ_{fd}), Anhysteretic Remanence (ARM) (respectively, anhysteretic susceptibility χ_{ARM}=ARM/h) and Isothermal Remanence (IRM) (Thompson and Oldfield, 1986). Exactly those parameters are characterized by data distributions, close to Gausian (normal) with skewness and kurtosis lower than 1 (Table 1).

Magnetic parameter	**N**	**average**	**Median**	**Min.**	**Max.**	**Std. Dev.**	**skewness**	**kurtosis**
χ (10^{-8} m^3/kg)	177	189.6	205.3	9.7	518.9	108.2	0.03	-0.66
χ_{fd} (10^{-8} m^3/kg)	177	14.9	15.5	0.4	39.7	8.7	0.24	-0.59
χ_{fd}%	177	8.3	7.8	2.3	16.1	2.5	0.94	1.45
IRM (10^{-6} Am^2/kg)	177	16.2	17.9	0.8	42.6	9.5	-0.07	-0.81
χ_{ARM}(10^{-8} m^3/kg)	177	976.9	1065.0	47.4	2331.1	549.5	-0.16	-0.78
χ_{arm}/χ	177	5.1	5.2	2.8	9.3	1.0	0.08	1.17
χ_{arm}/χ_{fd}	177	68.7	65.1	18.3	287.0	34.0	2.88	14.32
χ_{arm}/IRM_{2T} (10^{-5} mA^{-1})	177	0.6	0.6	0.3	1.4	0.2	1.86	5.67
S-ratio	177	0.8	0.9	-0.07	1.0	0.3	-1.95	2.67
IRM_{2T}/χ	177	0.08	0.08	0.03	0.15	0.02	0.07	1.17
HIRM ($10^{-6}$$Am^2$/kg)	177	739.94	700.00	75.00	2400.0	320.65	1.15	3.92

Table 1. *Descriptive statistics for the magnetic parameters and ratios of the collection analyzed. Average, median, maximum (max) and minimum (min) values for the magnetic parameters are shown, together with the standard deviation of the average (St. Dev.), skewness and kurtosis.*

This allows using them without additional transformations in the following statistical evaluation (Factor- and Cluster analyses). Magnetic susceptibility of the samples varied across a wide range – between (9.7 – 518.9)×$10^{-8}$$m^3$/kg, thus evidencing broad concentration gradient in the content of the strongly magnetic Fe-minerals. Similar extensive variations are

obtained for ITM_{2T} and χ_{ARM} (Table 1) as well. The other parameters, included in Table 1 are ratios, sensitive to changes in the grain size of the magnetic carriers in case of uniform (constant) mineralogy. Except the ratio χ_{arm}/χ, the rest of the parameters are non-normally distributed, suggesting the presence and overlapping of different populations. In order to use these parameters in the statistical analyses, requiring normal data distribution, log-normal transformation has been applied to the ratios χ_{arm}/χ_{fd}, χ_{arm}/IRM_{2T} , IRM_{2T}/χ and $HIRM/\chi$ after which skewness and kurtosis decreased, allowing these parameters to be included in further statistical treatment. The S-parameter, defined as $S=IRM_{0.3T}/IRM_{2T}$ reflects the relative contribution of high-coercivity magnetic minerals to IRM_{2T} and needed an exponential transformation in order to fit the normal distribution. The high-coercivity part of IRM, defined by HIRM parameter (Liu et al., 2007) (HIRM=0.5*(IRM2T-IRM0.3T)) had to be transformed by square-root function in order to display a normal distribution.

Factor analysis was performed in order to reduce the number of variables, explaining the variability in the data set and allowing a correct choice of independent variables for the subsequent cluster analysis. The results from the Factor analysis are shown in Table 2. Using as input variables the parameters listed in Table 1, the analysis revealed that four factors account for explanation of 94% of the total variability in the data set. The first factor accounts for 48% of the total variability. The highest contribution to this factor give concentration-dependent magnetic parameters (χ,χ_{fd}, ARM, IRM, χ_{arm}). The second factor explains 23% of the variability with ratios χ_{arm}/χ, $Ln(\chi_{arm}/\chi_{fd})$ and χ_{fd}% having the highest loadings to this factor. The third factor explains 13% of data variability with the major contribution from the ratio χ_{arm}/IRM_{2T}. The fourth factor explains 10% of the data variability and is dominated by the hard-coercivity remanent magnetization HIRM (Table 2). The obtained grouping of the variables, contributing the most to the three factors reflects their genetic relations to a certain grain size and magnetic mineral phase. The highest loading in Factor 1 has mass specific magnetic susceptibility (χ), revealing the major role of the concentration of strongly magnetic mineral phases to the total magnetic signal of the samples studied.

Factor	**Eigenvalue**	**% of the total variance explained**		**Cumulative %**
1	5.721	47.67		47.67
2	2.766	23.05		70.72
3	1.570	13.08		83.81
4	1.260	10.50		94.31
	Factor Loadings (Varimax normalized)			
	Factor 1	**Factor 2**	**Factor 3**	**Factor 4**
χ	**0.987**	0.063	0.032	0.083
Ln(HIRM/χ)	**-0.827**	-0.162	0.089	0.513
χfd ($10^{-8}m^3$/kg)	**0.942**	-0.160	-0.183	0.108
χfd%	-0.250	**-0.781**	-0.420	0.039
IRM (mAm^2/kg)	**0.927**	0.255	0.194	0.083
χ_{arm} ($10^{-8}m^3$/kg)	**0.946**	0.238	-0.045	0.114
χ_{arm}/χ	0.097	**0.866**	-0.405	0.049
IRM2T/χ	-0.004	0.695	0.628	0.076
Ln(χ_{arm}/χ_{fd})	0.191	**0.957**	0.081	-0.002
Ln(χ_{arm}/IRM_{2T})	0.081	-0.002	**-0.988**	-0.053
Exp(Sratio)	**0.805**	0.401	-0.067	-0.274
Sqrt(HIRM)	0.080	0.060	0.048	**0.976**

Table 2*. Results from the Factor analysis. Eigenvalues and explained variance for factors, determined using principal components extraction method (upper panel). Varimax-normalized factor loadings of different variables are in the lower panel. Loadings higher than 0.7 are indicated in bold.*

Although the bulk susceptibility is a sum of contributions of all minerals in the sample (paramagnetic, diamagnetic and ferromagnetic phases), magnetite-like fractions have χ-values one order of magnitude higher than the other phases, thus dominating the signal (Hunt et al., 1995). This is also proved by the high loadings to factor 1 of the other concentration-dependent magnetic parameters, in which, however, only the ferromagnetic (ferri- and antiferro) fractions contribute. The variables, determining 23% of the variability through Factor 2, are those related to the presence and quantity of the fine (nm-sized) single domain (SD) and superparamagnetic (SP) ferrimagnetic grains of magnetite (maghemite). Usually these magnetic fractions are related to soil development and/or firing (Taylor et al., 1987; Maher and Taylor, 1988), thus allowing discrimination of samples, most strongly affected by such processes. The magnetic parameter, which has the highest loading in Factor 3 is the ratio χ_{arm}/IRM_{2T} (Table 2). It is regarded generally as a proxy for the relative abundance of the stable single-domain ferrimagnetic grains if mineralogy is unchanged (Walden, 1999), while

the HIRM is solely related to the presence of iron (oxy)hydroxides hematite and goethite (Liu et al., 2007).

Thus, the four variables - χ, Ln(χ_{arm}/χ_{fd}) , Ln(χ_{arm}/IRM_{2T}) and sqrt (HIRM) were used as input data for running k-means cluster analysis using Statistica 6.0 software. We have utilized 100-folds cross-validation algorithm in order to choose the best number of clusters.

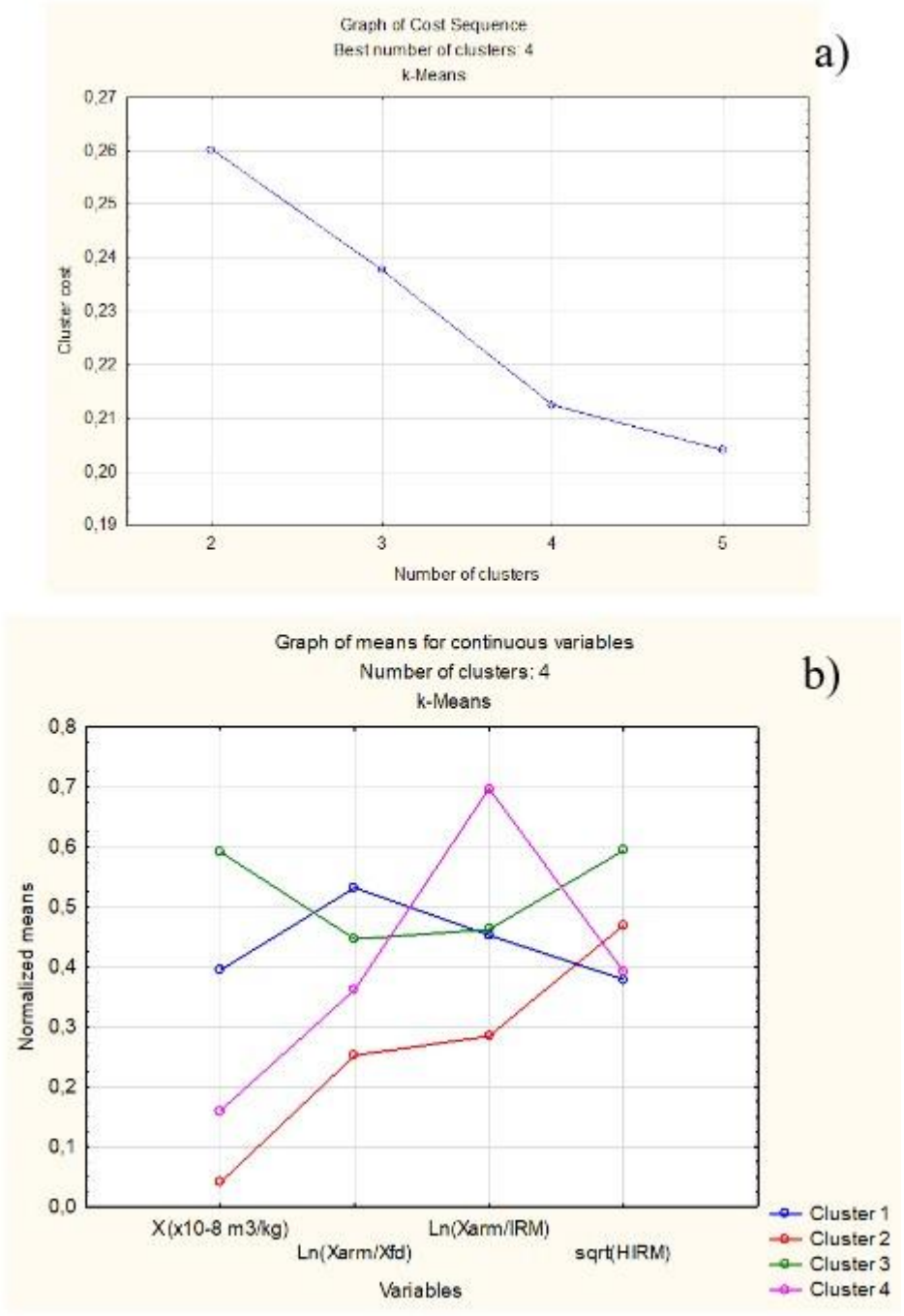

Figure 3. *Graph of cost sequence for determination of the best number of clusters (a) and graph of means of continuous variables (b) used for k-means cluster analysis.*

The obtained cost sequences (Fig.3a) shows that four is the best number of clusters, after which the cluster cost levels off and higher number of clusters does not contribute to the clustering. The normalized cluster means for the input continuous variables are presented in Fig. 3b. The calculated cluster means are well separated except the obtained smaller differences in the mean sqrt(HIRM) values for the clusters 1 and 4. K-means clustering algorithm (177 cases, training error 0.2) assigned each case (e.g. sample) to a certain cluster, which resulted in the following distribution of samples among the clusters: in cluster 1 – 83 samples, in cluster 2 – 25 samples; in cluster 3 – 41 samples; in cluster 4 – 28 samples. The distribution of samples among the clusters with the corresponding distances to the clusters' centroids is provided in Supporting Information.

2.2. Mineral magnetic signature of samples conforming to the four clusters

2.2.1. Magnetic minerals identification through high-temperature thermal behavior of magnetic parameters

Representative examples of step-wise thermal demagnetization of composite IRM for samples belonging to the four established clusters, are shown in Fig. 4 a-d. Strongly magnetic low-coercivity phase with T_{ub} of ~580°C dominates in samples from cluster #1 (Fig.4a). The other high-coercivity component (diamonds) is weak and gives insignificant contribution to the IRM signal. It unblocks progressively to 700°C. Similar behavior is observed for samples from cluster #4 (Fig. 4d), with an additional relatively weak high-coercivity component with T_{ub} of 250°C. This phase is also evident in cluster #3 (Fig. 4c). A very high amount of high-coercivity magnetic phases with T_{ub} of 100°C and 700°C are present in samples from cluster #2 (Fig. 4b). Samples from cluster #4 show similar unblocking temperatures to that of the clusters 1 and 3 with T_{ub} of 580°C and T_{ub} of 250 - 270°C on the high-coercivity component.

Continuous monitoring of the high-temperature behavior of magnetic susceptibility (thermomagnetic analysis, k-T) is another widely used experimental approach in mineral magnetism for identification of ferromagnetic minerals through their Curie/Neel temperatures (Dunlop and Özdemir, 1997). Some examples of k-T curves are shown in Fig. 4e-h. Sample A61 from cluster 1 shows strong mineralogical changes upon heating, since the cooling curve displays much stronger signal compared to the initial heating (Fig. 4e). On the heating curve a clear bump is observed at ~300°C, followed by sharp decrease in k until ~400°C and a well expressed final decrease to 580°C.

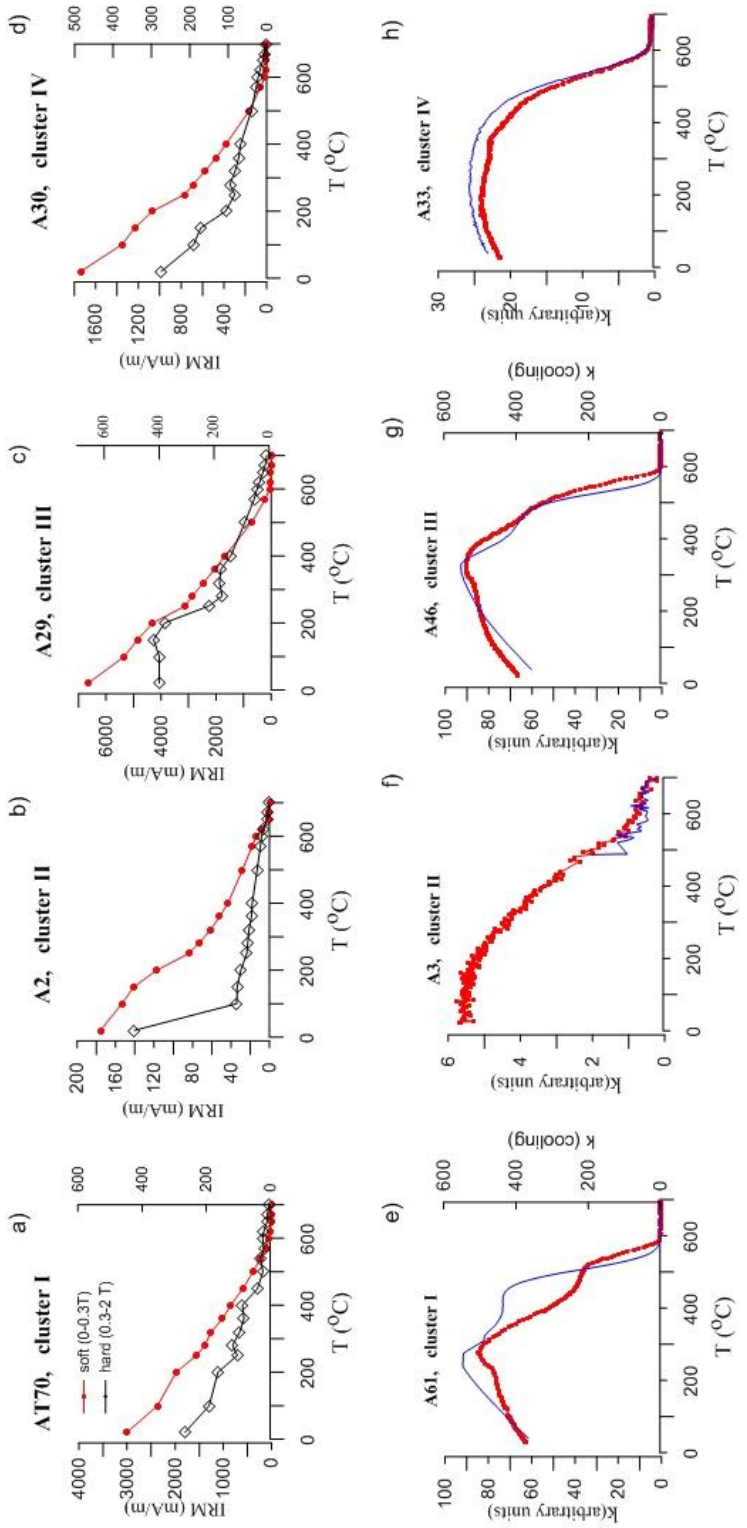

Figure 4*. Examples of step-wise thermal demagnetization of composite IRM (Lowrie, 1990) for representative samples from each cluster (a-d). Examples of the high-temperature behavior of the magnetic susceptibility for samples from each cluster (e-h). Red dotted line represents heating run, black thin line – cooling run. Heating and cooling performed in air. Heating rate: 11°C/min.*

The sample from weakly magnetic cluster #2 shows a convex curve with final drop of magnetic susceptibility at 700°C. The sample from cluster #3 shows moderate increase in k up to ~300°C, followed by sharp decrease and diminishing signal at 600°C (Fig. 4f), similarly to sample A61 from cluster #1 (Fig. 4e). Significant mineralogical transformation occurs during laboratory heating, since magnetic susceptibility increases significantly on cooling (note the separate axis for the cooling curve on Fig. 4g). Sample A33 belonging to cluster #4 displays convex heating curve with a small bump at ~400°C and a final drop in susceptibility at ~580°C (Fig. 4h). In contrast to the sample from cluster #3 (Fig. 4g), the cooling curve for sample A33 is almost reversible (Fig. 4h).

2.2.2. Magnetic minerals identification through step-wise acquisition of Isothermal Remanent magnetization (IRM) and coercivity components decomposition

Step-wise acquisition of IRM was carried out for 14 samples selected from the four clusters. The acquisition curves obtained were processed with the MAX UnMix software (Maxbauer et al., 2016) in which IRM spectrum is analyzed using distribution of cumulative Gaussian functions (Robertson and France, 1994; Kruiver et al., 2001; Egli, 2004). Each IRM component is characterized by its relative contribution to the total IRM (% contr.), the field at which half of the SIRM is acquired ($B_{1/2}$, given in log-units, as well as in "mT"), and the width of the distribution, expressed through the dispersion parameter DP (one standard deviation of the logarithmic distribution) (Kruiver et al., 2001). Representative examples for the IRM acquisition curves and the coercivity distribution fitting are shown in Fig. 5.

IRM acquisition curves for the samples from cluster #1 were fitted by three components – one with the lowest coercivity, varying between (3-10) mT, a second one with $B_{1/2}$ in the interval (24-27) mT, and a third one with coercivity in the range (268-1494 mT) (Table S_1 from the Supporting Information). The highest contribution to the total IRM comes from the second component, while the softest and the hardest ones contribute relatively little (Fig. 5a, Table S_1 from Supporting Information). Acquisition curves obtained for the samples from the second cluster are also fitted by three components, but the softest one, isolated in samples from cluster #1 is not present. Instead, the third component of very high coercivity ($B_{1/2}$ in the interval (4000 - 7700) mT is identified (Fig. 5b). It is noteworthy that this component accounts for large part of the total IRM – up to 41% (Table S_1 from Supporting Information). The components 2 and 3 have the same coercivity as these ones for the samples from cluster #1.

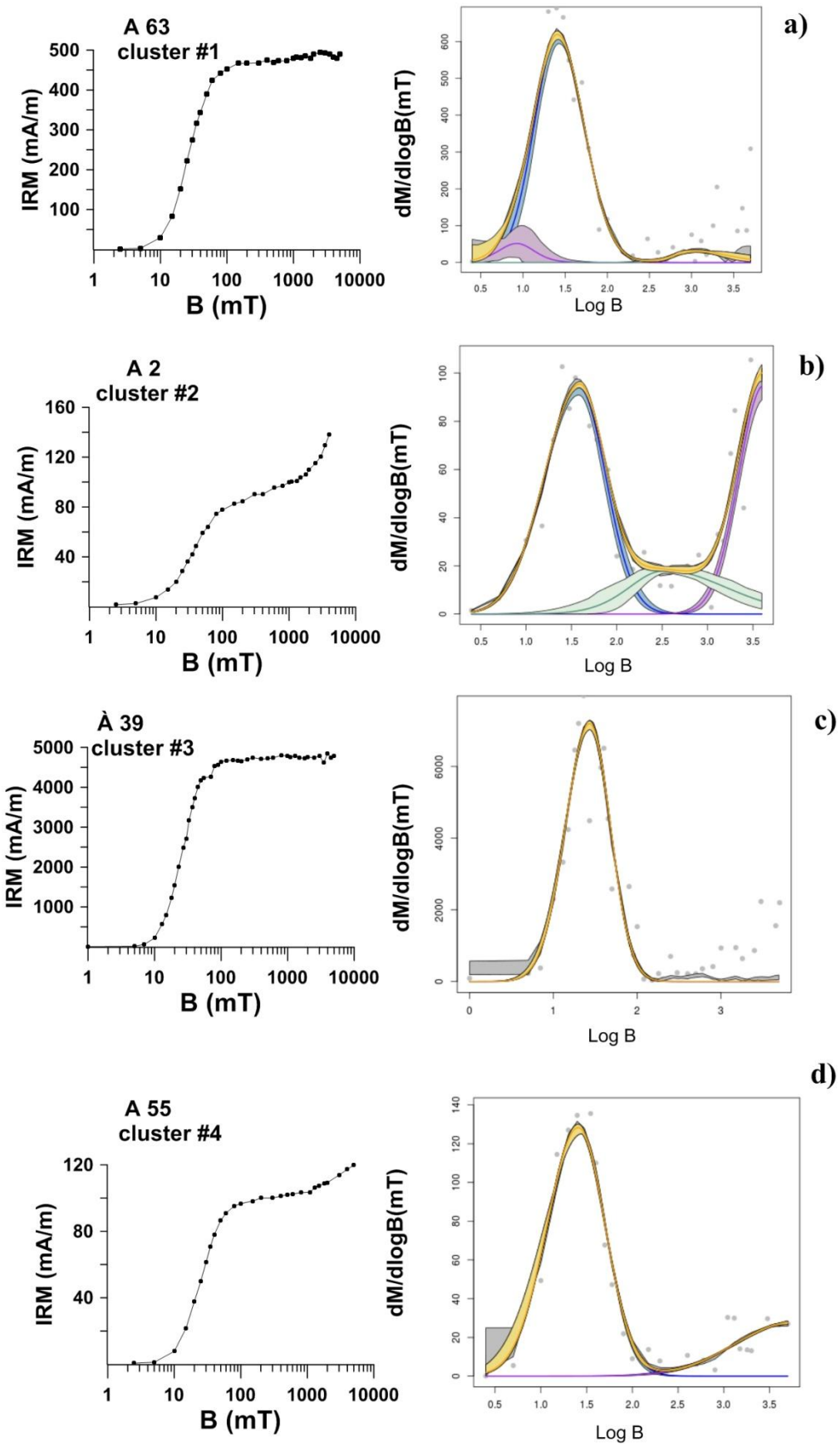

Figure 5. *Examples of IRM acquisition up to 5T field (left panel) and the unmixed coercivity components using MAX UnMix software by Maxbauer et al. (2016) (right panel). Data points are denoted by dots; cumulative fit together with its confidence band is shaded in yellow.*

The two samples from cluster #3 show very similar IRM acquisition curves in which the component with $B_{1/2}$ =27mT accounts for almost the whole remanent magnetization (Fig. 5c). Samples from cluster #4 also show the dominant contribution of the IRM component with $B_{1/2}$ in the interval (24-27) mT, while components 3 and 4 make various weak contributions in the three curves (Table S_1 from Supporting Information, Fig. 5d).

2.2.3. Major magnetic characteristics of samples from the four clusters

Figures 6-7 represent the box-and-whisker plots of the main magnetic parameters of the samples from each cluster. Median, upper- and lower quartiles are shown. The samples with the highest magnetic susceptibility (χ) are grouped in clusters 1 and 3 (Fig. 6a), the same having also the highest values of isothermal remanence (IRM_{2T}) (Fig. 6b), as well as of anhysteretic susceptibility (χ_{arm}) (figure not shown). Samples from clusters #2 and #4 have low values of χ and IRM_{2T}. The presence of high-coercivity minerals, as deduced by the parameter HIRM is shown in Fig. 6c.

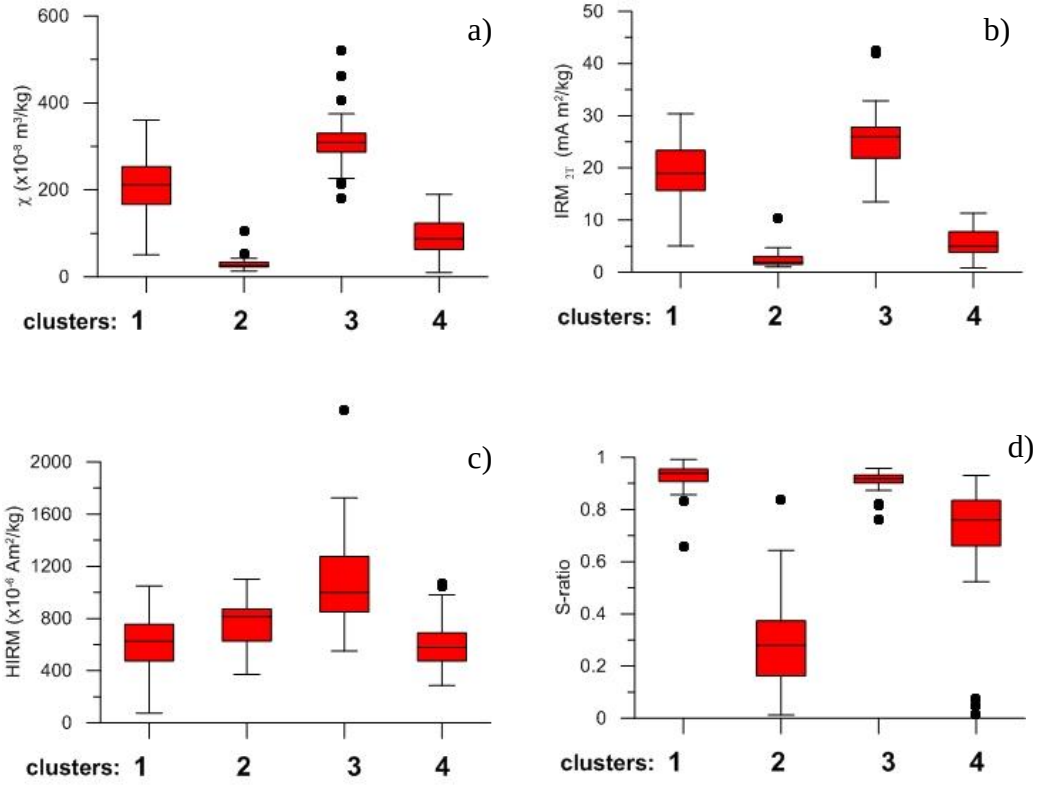

Figure 6*. Box-and-whisker plot of concentration-dependent magnetic parameters magnetic susceptibility (χ) (a), isothermal remanent magnetization (b), HIRM (c) and the S-ratio (d) for the samples, belonging to the four clusters. Median, upper- and lower quartiles are shown.*

The outliers are defined as having values higher than 1.5 times the Inter-quartile-range (IQR) of the corresponding data distribution and are represented by dots.

This parameter reveals increasing amount of hard coercivity fraction from clusters #1 to #3, and HIRM for cluster #4 is similar to that one for cluster #2. The relative contribution of this hard fraction to the total IRM, revealed by the S-ratio shows that clusters #1 and #3 contain samples with dominant magnetically soft minerals, since S-ratio is close to 1 (Fig. 6d). In contrast, cluster #2 contains samples with very low S-ratios, suggesting important contribution from hard coercivity fractions. Cluster #4 includes samples with intermediate S-ratio values, varying between 0.5-0.9 (Fig. 6d).

Grain-size related magnetic parameters are presented in Fig. 7. Percent frequency dependent magnetic susceptibility χ_{fd}%, reflecting the relative contribution of the finest nanometer-sized particles of iron oxides shows relatively high values in all four clusters and a trend of overall increasing χ_{fd}% from cluster #1 towards cluster #4 could be inferred (Fig. 7a). The ratio χ_{arm}/χ_{fd}, depicting the relative importance of stable single-domain (SD) as compared to the finest superparamagnetic grains (expressed by χarm and χ_{fd}, respectively), shows its maximum values in cluster #1, while in cluster #2 it is at minimum (Fig. 7b). The ratio χ_{arm}/IRM_{2T}, sensitive to the presence of stable single domain ferromagnetic grains (grain sizes of about 15-20 nm) (Thompson and Oldfield, 1986; Dunlop and Özdemir, 1997) also posses the highest values in cluster 4, while minimum values are obtained for samples from cluster #2 (Fig. 7c). Another magnetic ratio used in this study, is IRM_{2T}/χ, meant to represent the relative share of remanence-carrying fraction in the total mineral content, as reflected by the magnetic susceptibility (Thompson and Oldfield, 1986). As it is seen from Fig. 7d, this ratio has maximum values for samples from cluster #1, while for the other three clusters it is progressively smaller.

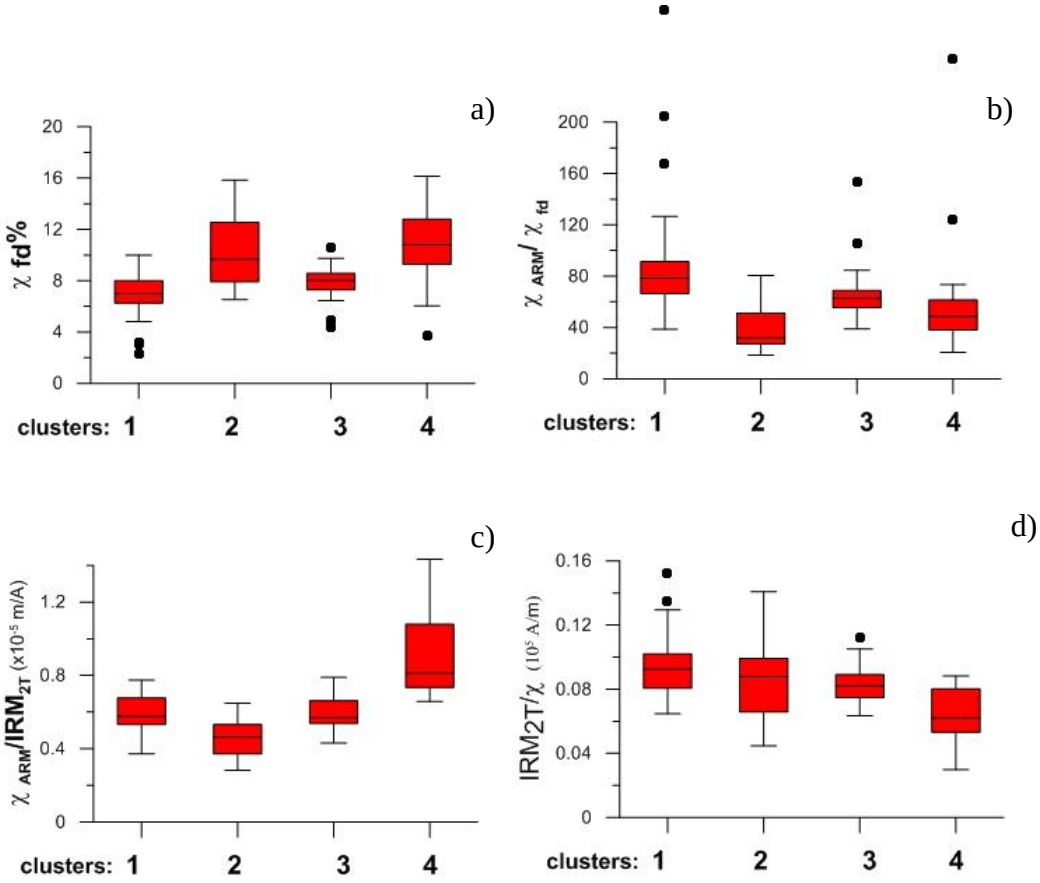

Figure 7*. Box-and-whisker plot of percent frequency-dependent magnetic susceptibility (χ_{fd}%) (a), and magnetic ratios: $\chi_{ARM}/\chi fd$ (b); χ_{ARM}/IRM (c) and IRM_{2T}/χ (d). See the text for details. Median, upper- and lower quartiles are shown. The outliers are represented by dots.*

3. Discussion

3.1. Magnetic minerals identification

Thermal methods utilized for identification of the magnetic minerals, responsible for the magnetism of materials collected from Ada Tepe ancient gold mine were used for determination of the Curie- and unblocking temperatures of the magnetic phases. The main magnetic mineral showing unblocking temperature around 580°C on the magnetically soft IRM component in all samples (Fig. 4) and having Curie temperature T_c=580°C is magnetite (Dunlop and Ödemir, 1997). Unblocking of soft remanence component at ~200°C (Fig. 4b, c, d) could be due to grain-size effect, since coarse magnetite/maghemite particles have lower T_{ub}. Magnetically hard component with T_{ub}~700°C seen in all samples (Fig. 4) is identified as hematite, while sharp drop in hard IRM at ~100°C for the sample from cluster #2 (Fig. 4b) can be ascribed to goethite (Dunlop and Ödemir, 1997). As far as the saturation remanences of the latter two minerals are order of magnitude lower than that of magnetite, their clear

presence in the hard IRM component shows that significant part of the magnetic mineralogy is represented by goethite and/or hematite (Frank and Nowaczyk, 2008; Dunlop and Özdemir, 1997). The identification of goethite in samples from cluster #2 unambiguously points that these materials did not undergo heating in the past as a result of ancient mining and/or other anthropogenic activities, as far as goethite is thermally unstable and transforms to hematite when heated to higher temperatures (Dekkers, 1988). Unblocking temperature T_{ub}~250°C, observed on the hard IRM component in samples from clusters #1,#3 and #4 can be linked except to grain size effect of unblocking coarse magnetite grains, also to the presence of pyrrhotite which transforms upon heating to magnetite and may be a reason for the strong increase in magnetic susceptibility on cooling curves of the thermomagnetic analysis (Fig. 4a, c). Partly this strong magnetic enhancement could be due to mineral transformations of the initial clay fraction of the material, which is thermally unstable upon heating. Many studies (Murad and Wagner, 1988; Bruhns and Fischer, 2001, Dionisio et al., 2009) show the appearance of new magnetic fraction (mainly magnetite) as a result of heating kaolinitic clays, clays rich in montmorillonites, etc. Another source of strongly magnetic fraction after heating soil material are the transformation products of weakly magnetic iron oxyhidroxides (lepidocrocite, goethite, ferrihydrite), usual end-products of surface weathering reactions (Cornell and Schwertmann, 2003).

IRM acquisition curves and their decomposition into coercivity components (Table S_1 from Supporting Information, Fig. 5) lead to consistent results, demonstrating the prevailing contribution of magnetite-like component with coercivity $B_{1/2}$ ~ 25mT in all samples. This is in support of the idea that magnetite is inherited from the parent rocks in the study area. Similar conclusion is reported in Ajdanlijsky et al. (2008). The softest magnetic component with $B_{1/2}$ ~ 8mT is present only in samples from cluster #1 and could be ascribed to the occurrence of very fine-grained magnetite grains at the SP/SD magnetic grain size boundary (Dunlop and Özdemir, 1997). IRM component 3 with $B_{1/2}$ ~ 700-1000 mT, corresponding to hematite (Kruiver et al., 2003) is more important in samples from clusters #1 and #2 (Table S1 from Supporting Information) and has much lower coercivity and relative share in IRM in samples from clusters #3 and #4.

Synthesizing the information obtained from the magnetic minerals diagnostic methods above, it could be concluded that the following magnetic minerals are present in the samples from the four clusters:

i) cluster #1: magnetite/maghemite and hematite

ii) cluster #2: goethite, hematite, magnetite (minor amount)

iii) cluster #3: magnetite, pyrrhotite, hematite

iv) cluster #4: magnetite, hematite, (?pyrrhotite), goethite (rare)

3.2. Cluster's members

Samples from the cluster #2 are characterized by magnetic behavior, very contrasting to the other groups of samples. Except significantly lower concentration of the strongly magnetic fraction (Fig. 6) these samples exhibit very different magnetic mineralogy, as revealed by the low values of the S-ratio (Fig. 3d) and high amount of iron oxyhydroxide goethite detected (Fig. 5b, Table S_1 from Supporting Information). Despite the low values of χ, samples from cluster #2 show high χ_{fd}% (Fig. 7a). This apparent discrepancy could be due to the dominant presence of fine SP-hematite, which displays anomalously high χ_{fd}% (Wells et al., 1999). Majority of the samples in cluster #2 is described in the field book as coming from the host rock (Supporting Information) which is confirmed by the magnetic analyses. The presence of Fe-hydoxide is characteristic for the weathering of rocks and sediments (Cornell and Schwertmann, 2003) and is also proved by the mineralogical studies of Ada Tepe host rocks (Tsintsov et al., 2016). Thus, we hypothesize that cluster #2 is composed of materials from the natural host rocks.

Samples, included in cluster #3 show the highest magnetic enhancement, as expressed by magnetic susceptibility and IRM (Fig. 6a, b), the strongest HIRM among the clusters (Fig. 6c), which however is obviously due to moderately high-coercivity mineral, as evidenced by the relatively high S-ratio (Fig. 6d) and the decomposition of IRM acquisition curve (Table S_1 from Supporting Information). Grain-size sensitive magnetic parameters (Fig. 7) show that samples from this cluster contain moderate amount of SP fraction (χ_{fd}%~8%; Fig. 7a), as well as remanence-carrying SD fraction (Fig. 7c, d). Except as a common product of pedogenic development, strongly magnetic fraction consisting of SD and SP magnetite-like grains is also characteristic of soils/sediments which experienced burning (Longworth et al., 1979; Vendelboe et al., 2005; Jordanova et al., 2019). On the other hand, natural soils usually show much lower natural pedogenic magnetic enhancement (Jordanova, 2016). This high enhancement can be due to strongly magnetic parent rocks (Lu et al., 2008) but it is not the case with Ada Tepe site, where host rocks are weakly magnetic (cluster #2). Therefore, it can be supposed that majority of the materials belonging to cluster #3 are burnt sediments/soils and heap material from rock processing with the use of fire.

Magnetic parameters and grain-size dependent ratios for samples, belonging to cluster #4 all conform to the values, commonly observed in natural soils (Jordanova et al., 2016) and in particular Luvisols (Maher, 1986; Torrent et al., 2010; Jordanova, 2016). Magnetic susceptibility does not exceed χ~100-150 $\times 10^{-8} m^3/kg$ (Fig. 6a) and the highest median χ_{fd}% is observed for this cluster (Fig. 6a), suggesting a very important share of SP magnetite fraction. Comparison between the obtained cluster's members and the field description (Supporting Information) shows that cluster #4 is composed largely of samples from brown and brown-red soils, soils close to archaeological structures, as well as some yellowish layers, probably belonging to soils' BC horizons.

The cluster #1 encompasses samples showing similar to cluster #4 (natural soils) concentration-dependent magnetic parameters but with higher proportion of the stable SD fraction, leading to the highest median χ_{arm}/χ_{fd} among the clusters (Fig. 7b). This observation, along with the highest range of the IRM_{2T}/χ ratio (Fig. 7d) shows that the stable remanence-carrying fraction dominates in these materials, while the superparamagnetic component is less significant. Such situation is often observed in fired soils, where stable SD fraction increases as a relative contribution in the bulk magnetic mineralogy (Jordanova et al., 2019). Therefore, we attribute cluster #1 to fired soils (archaeological structures, burned soils, etc.). Comparison with the field notes (Supporting Information) shows that majority of materials from cluster #1 are described as soils from cultural layers, archaeological structures, reddish layers with charcoals. There are also samples, distinguished as brown-reddish heap material, which were tentatively linked to the cluster #3 (as described above). This mixing is not surprising, taking into account the fact that magnetic susceptibility for cluster #1 varies in a wide interval, incorporating also the range of values, characteristic for cluster #4 as well (Fig. 6a).

3.3. Environmental implication of mineral magnetic data from the Ada Tepe ancient gold mine

Archaeological site at Ada Tepe (Krumovgrad, South-Eastern Bulgaria) has markedly complex characteristics which require utilization of diverse interdisciplinary methods in addition to classical archaeology. Only such integrative approach is able to provide reliable analysis and interpretation of the field- and laboratory analytical data to reconstruct the ancient human activities during the second half of the II^{nd} millennium B.C. An important constituent of the complex data base is the information and artifacts, collected during the field

567 excavations of the ancient mining, ore-processing and related human activities at the ridge
568 and the elevated slopes of Ada Tepe hill.
569 The identified magnetic mineralogy of materials from Ada Tepe gold mine, tightly
570 related to the forms and amount of Fe-(oxy)hydroxides, reflects the changes in mineralogical
571 composition of different parts of the deposits. Supergene processes lead to strong oxidation in
572 the uppermost parts of the Ada tepe deposits, resulting in pyrite oxidation and formation of
573 goethite (Marchev et al., 2004). Thus, largely present goethite in the samples from the cluster
574 #2 is most probably related to the wastes of ancient mining of such highly oxidized deposits,
575 which however is shown to be poor in Au enrichment (Marchev et al., 2004). Identified
576 pyrite/pyrrhotite in the samples from clusters 2, 3, and 4 are related to the mining/exploitation
577 of the ore deposits from the hydrothermally affected host rocks, containing the electrum
578 (Tsintsov et al., 2016). The use of fire as an ancient mining technology during pre-historic and
579 later times is well documented in different places (Weisgerber and Wilies, 2000; Heldal and
580 Storemyr, 2015). The use of fire as a technology in locations of the samples from cluster #3 is
581 fully supported by the magnetic data, indicating absence of unstable Fe oxyhydroxides
582 (goetite) and the highest abundance of secondary magnetic minerals. The presence of
583 magnetite as magnetic component in all samples (Table 1S from Supporting Information) is
584 probably related to the mineralogy of the host rocks (Ajdanlijsky et al., 2008), but it may be
585 also a product of pyrite alteration, as well as by-product of goethite thermal transformation
586 (Özdemir and Dunlop, 2000). Magnetic signature of materials, classified in cluster #1 is
587 distinguished from the others by the presence of a magnetic component with very low
588 coercivity (Fig. 5a, Table 1S from Supporting Information) which can be attributed to sub-
589 micron magnetic fraction consisting of unstable grains at the SP/SD domain boundary,
590 produced during firing of soils at the various archaeological structures. Taking into account
591 that more prolonged firing produces larger grains than shorter and/or single burning (Long et
592 al., 2016), it can be supposed that heap materials from mining operations with fire settings,
593 classified in cluster #3 were treated by prolonged firing. In contrast, materials from cluster #1
594 showing magnetically softer behavior belong mostly to archaeological features (burnt soil
595 close to fireplace, etc.) which might be heated to lower temperatures and/or for a shorter time.
596
597 Spatial distribution of sampling locations, grouped in the four clusters according to
598 their rock-magnetic characteristics, is shown in Fig. 8. Analysis of magnetic mineralogy of
599 the samples grouped in the four clusters, together with their spatial distribution (density and
600 topographic allocation) in the various areas on the slopes and the hilltop of Ada Tepe, allow

drawing conclusions related to the degree of human impact on the environment, the organization of the working process and the whole *chaîne opératoire* of the ore exploitation during the Late Bronze age epoch.

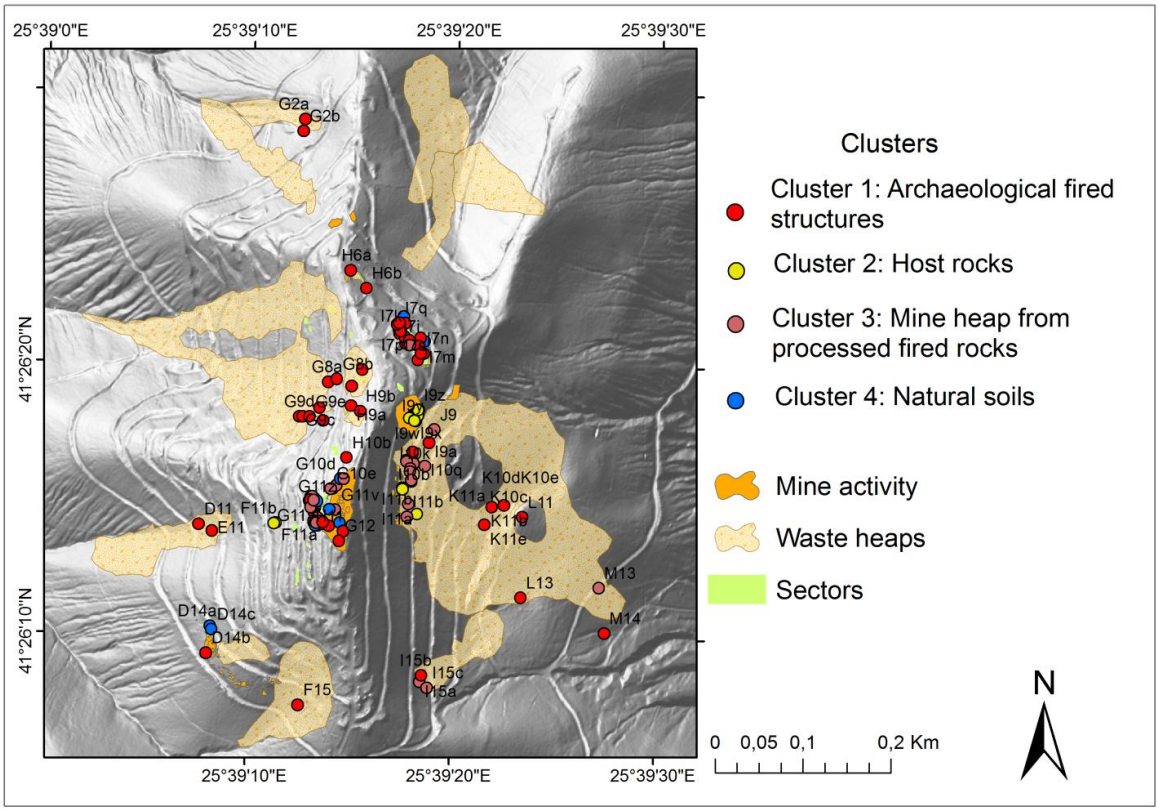

Figure 8. *Spatial distribution of samples separated in the four clusters.*

Samples classified in cluster #1 as archaeological fired materials are the most spread and are found in all sectors where human activities are detected. Fired archaeological features confirm the wide influence of the ancient mining over the whole hill. Samples belonging to this cluster are the most numerous and are abundant both in the waste heaps along the slopes of the hill, and in the area of the two settlements and the working stages located in the northern parts of the hilltop and the elevated parts of the western slopes of Ada Tepe (Fig. 8). Noteworthy, in the area of the working stages for ore-processing in sectors G-8, G-9, H-6, H-9, H-10 samples classified in cluster #1 are exclusively found. Two hypotheses could be suggested for explanation of this picture: 1) At this part of the hilltop of Ada Tepe for the long-term period ore processing (crushing and grinding) had taken place. Probably, the ore fragments have been initially treated in a fire-setting during the previous phases of ore

processing; 2) Fire-setting had been also applied during the process of ore processing and crushing. One of the hypotheses does not exclude the other one, but the classification of samples in the above mentioned sectors is remarkable. Longstanding accumulation of the technological waste, related to the use of fire-setting strongly influenced this part of the hilltop. Large portion of the samples from cluster #1 which are spread on the slopes of the waste heaps (Fig. 2) at the lower parts of the hill maybe associated with the active processes of erosion and re-settling. Such hypothesis is logical taking into account the fact that mining and metallurgy cause deforestation and denudation. Denudation processes can be related to the working operations and gravitational settling of the waste materials thrown by the ancient miners down-slope, as well as to the natural erosion processes through time after the end of the gold mining. As a result of the human activities and the natural processes, the spatial distribution of the materials with fire-affected magnetic characteristics covers the entire elevated part of the hill above ~340-350 m a.s.l.

Samples from cluster #2, identified as host rocks, are agglomerated in the areas defined by the archaeological evidences as mining areas (Fig. 8), as well as in the waste heaps at the eastern slopes of the hill. Remarkably. materials assigned to cluster #2 are concentrated mainly in sectors where parts of the open gold mine (sectors I-9.I-10, I-11, J-9) exploited at the eastern slopes of the hill were discovered. Lack of changes in magnetic phases related to thermal processes links these materials to the host rocks, which are depleted in ore content and are not influenced by the fire-setting during the primary ore mining. In the above mentioned sectors samples collected belong to different clusters (#1, 2 and 3), characterized by various magnetic mineralogy. This diversity can be due to the fact that fire-setting in the mining sectors has not been applied everywhere on the whole area, but rather after identification of the parts of the host rock where ore veins were discernible as perspective. The fire setting had been applied locally and selectively in order to save time and resources. Ore-deficient rocks were not processed, but gold mineralization profitable for standards was present practically in the whole sedimentary complex of the ore deposit.

Materials, identified through their rock-magnetic characteristics as representing mine dump from mining with the use of fire (cluster #3) are found mainly on the eastern slopes of Ada Tepe (sectors I-9, I-10, I-11, I-15, Fig. 8). Samples from this cluster are mainly spread in the sectors where direct ore mining was done, or in the elevated parts of the waste heaps. They are not spread far below the slope, as it is the case with big part of the materials classified in cluster #1 (Fig. 10). The only exception along the eastern slopes is a sample in the sector M13 located in the eastern shallow periphery of the big heap. Another sector with

high concentration of samples belonging to cluster #3 is located at the western periphery of the hilltop (sector G-11). There the most intense and advanced mining technology was registered in the Late Bronze Age (e.g. ~ XVth century B.C. (Popov et al., 2017). Large number of samples from cluster #3, located at the western periphery of the settlement existing at the hilltop is surprising at first glance, but could be easily explained taking into account that the hill's cover is in fact the first mining area where the gold mining had started in the middle of the second millennium B.C. As a result of the hill's destruction an ellipsoidal platform appeared where the settlement was later founded and developed during several phases. Samples from cluster #3 in sector G-11 are situated exactly at the periphery of the former ore-mining platform. Major part of these strongly altered by fire rock pieces are left close to the production place. They are later re-used as building material in the fortress wall's foundation from the end of the XIIIth century B.C. or in the rock basement of some of the buildings at that place. The presence of samples from cluster #3 in sector I-7 could be related to the small local ore extraction along single ore veins, separated from the richest and long-exploited by the mining activities ore deposits.

Natural soils (cluster #4) are only occasionally found in the northern parts and on the hilltop (Fig. 8). This cluster contains the smallest number of samples in spite that sampling was done regularly across the sectors. This fact evidences the large-scale influence of the active gold mining on the natural environment at Ada Tepe hill. Samples from cluster #4 are found only on the territory of the two settlements – the one at the north-eastern slopes (sector I-7) and at the hilltop (sectors G-11, G-12) (Fig. 8). At both places no traces of earlier ore-mining were detected and thus they have not been directly influenced by mining, in spite that in the neighboring sectors there are areas affected. An exception is the sample taken from sector D-14, located in the area of the mine gallery registered there. However, obviously this specific spot was not affected by the gold mining.

Experimental laboratory magnetic studies on the collection of samples from the Late Bronze Age gold mine Ada Ttepe reveal the potential of this type of investigations for systematic classification of the type of the materials, related to their thermal history and genesis. This goal is achieved due to the very high sensitivity of the forms and abundance of the different types of iron compounds and mainly Fe-oxides to the differences in the environmental conditions during their formation and subsequent diagenetic and/or anthropogenic alterations. Future aim will be to investigate the chemical and elemental composition, as well as the forms of the potentially toxic elements contained in the waste heaps and other materials from the ancient gold mining and will be a focus of another study.

Conclusions

Mineral magnetic study of a collection of materials from the ancient gold mine site at Ada Tepe revealed that rock-magnetic characteristics provide precise information about the kind of magnetic minerals, their relative abundance, grain size and thermal history. Statistical treatment of the data set using factor- and cluster analyses provided objective classification of materials, which is consistent with the major archaeological observations. Host rocks magnetic mineralogy is characterized by the dominance of goethite and hematite, along with a weak magnetite's component. Materials from waste heaps of processed rocks with fire setting are characterized by the strongest magnetic enhancement with predominant presence of magnetite and hematite. Materials from archaeological features from cultural layers also show enhanced magnetic properties, but dominated by very fine-grained magnetite, while hematite component is minor. Materials from natural soils were separated in a group exhibiting magnetic characteristics conforming to the already available data for Luvisols from Bulgaria. Thus, it can be concluded that mineral magnetic approach can be profitably employed as a sensitive, relatively fast and precise tool for characterization and classification of waste dumps from ancient mining activities. The combination of the mineral magnetic approach with the stratigraphic and conceptual information, collected during the conventional archaeological excavations, allows deriving much more detailed and specific conclusions related to the overall organization as well as characteristics of the different divisions in the technological chain for the exploitation of the ore deposit during the Late Bronze age.

Acknowledgements

This study is financially supported by the national co-financing for the Bulgarian team participating in COST Action CA17131 "The Soil Science & Archaeo-Geophysics Alliance: going beyond prospection (SAGA)", grant No KP-06-COST/2, funded by the Bulgarian National Science Fund. Field sampling of materials included in the study and their initial laboratory measurements were funded by the Financial contracts between the National Archaeological Institute with Museum (Bulgarian Academy of Sciences) and Dundee Precious Metals Ltd. (Krumovgrad) for: "Ada tepe Rescue archaeological surveys during the campaigns 2010-2013 and 2015" and "Processing of artifacts and materials uncovered by the rescue archaeological surveys along with the associated database and accumulated field and lab-based documents. Period 2015-2018". Raw data used for construction of graphs included in the paper and in Table S_1 are available in the Supporting Information and after acceptance

722 will be publicly available through Mendeley data repository (DOI reserved:
723 http://dx.doi.org/10.17632/88kx59c2rf.1).
724
725
726 References
727 Ajdanlijsky, G., Nehrizov, G., lieva, E., Zlatanov, D., 2008. Mineralogical peculiarities of the
728 heavy mineral fraction from sherds and sediments from the archaeological site “Ada
729 Tepe”, Kroumovgrad district. Geoarchaeology and Archaeomineralogy (Eds. R. I.
730 Kostov, B. Gaydarska, M. Gurova). 2008. Proceedings of the International
731 Conference, 29-30 October 2008 Sofia, Publishing House “St. Ivan Rilski”, Sofia, 83-
732 92.
733 Baron, S., Tămaș, C.G., Rivoal, M., Cauuet,B., Télouk, P., Albarède, F. 2019. Geochemistry
734 of Gold Ores Mined During Celtic Times from the North-Western French Massif
735 Central. Scientific Reports, 9(1),17816
736 Bruhns P. and Fischer R.X., 2001. Phase reactions in the brick firing process of V-doped
737 clay. Eur. J. Mineral., 13, 611 – 619.
738 Chapman, R., Leake, R.C., Warner, R.A., Cahill, M.C., Moles N.R, Shell, C.A., Taylor J.J.,
739 2006. Microchemical characterisation of natural gold and artefact gold as a toll for
740 provenancing prehistoric gold artefacts: a case study in Ireland. Applied
741 Geochemistry 21, 904–918.
742 Certini, G., 2005. Effects of fire on properties of forest soils: a review. Oecologia, 143, 1-10.
743 CORINE Land Cover (2018) [Online]. Available from: https://land.copernicus.eu/pan-
744 european/corine-land-cover/clc2018 [Assessed: 11/11/2020]
745 Cornell R. and Schwertmann, U., 2003. The Iron Oxides. Structure, properties, reactions,
746 occurrence and uses. Weinheim, New York.
747 Craddock, P. T., 1992. A short history of firesetting. Endeavour 16, 3, 145-150.
748 Craddock, P. T., 1995. Early metal mining and production. Edinburgh University Press, UK,
749 ISBN 0 7486 0498, 363pp.
750 Dekkers, M., 1988. Magnetic behaviour of natural goethite during thermal demagnetization.
751 Geophys. Res. Lett., 15 (5), 538 – 541.
752 Dimitrov K., Stoychev, K. 2018. The East Balkan Region as a Source of Precious and Non-
753 ferrous Metals from Prehistory to the Roman Period. In: S. Alexandrov, Y. Dimitrova,

754 H. Popov, B. Horejs, K. Chukalev (eds.), Gold and Bronze. Metals, Technologies and
755 Interregional Contacts in the Eastern Balkans during the Bronze Age. Sofia, 43-57.
756 Dionísio A., Braga M. A., Waerenborgh J.C., 2009. Clay minerals and iron oxides-
757 oxyhydroxides as fingerprints of firing effects in a limestone monument. Applied Clay
758 Science, 42, 629–638.
759 Domergue, C., 2008. Les mines antiques. La production des métaux aux époques grecque et
760 romaine. Picard, Paris (collection Antiqua), 240 pp
761 Dunlop D. and Özdemir, O., 1997. Rock Magnetism. Fundamentals and frontiers, ed. D.
762 Edwards, Cambridge Studies in Magnetism, Cambridge University Press.
763 Egli, R., 2004. Characterization of individual rock magnetic components by analysis of
764 remanence curves. 3. Bacterial magnetite and natural processes in lakes. Phys. Chem.
765 Earth, 29, 869–884.
766 Evans, M., Heller, F., 2003. Environmental Magnetism: Principles and Applications of
767 Enviromagnetics. Academic Press, San Diego, CA.
768 Frank U. and Nowaczyk, N.R., 2008. Mineral magnetic properties of artificial samples
769 systematically mixed from haematite and magnetite. Geophys. J. Int., 175, 2, 449-461.
770 Goranov, A. and Atanasov, G., 1992. Lithostratigraphy and formation conditions of
771 Maastrichtian-Paleocene deposit in Krumovgrad District. Geol. Balc., 22(3), 71–82.
772 Grogan, K., Gilkes R.J., Lotermoser B.G., 2003. Maghemite formation in burnt plant litter at
773 East Trinity, North Quinsland, Australia. Clays Clay Minerals, 51, 4, 390 – 396.
774 Heldal T. and Storemyr P., 2015. Fire on the Rocks: Heat as an Agent in Ancient Egyptian
775 Hard Stone Quarrying. In: G. Lollino et al. (eds.), Engineering Geology for Society
776 and Territory – Volume 5, pp. 291 – 295; DOI: 10.1007/978-3-319-09048-1_56,
777 Springer International Publishing, Switzerland.
778 Hunt, C.P., Moskowitz B.M., Banerjee S.K., 1995. Magnetic properties of rocks and minerals.
779 In: Rock physics and Phase relations. A handbook of physical constants. AGU
780 Reference shelf 3, pp. 189 – 204.
781 Jordanova, N. 2016. *Soil Magnetism. Applications in Pedology, Environmental Science and*
782 *Agriculture*. 1st Edition, Academic Press (Elsevier), 2016, ISBN:9780128092392, pp.
783 446.
784 Jordanova, N., Jordanova, D., Petrov, P., 2016. Soil magnetic properties in Bulgaria at a
785 national scale—Challenges and benefits. Global and Planetary Change, 137, Elsevier,
786 ISSN:0921-8181, DOI:10.1016/j.gloplacha.2015.12.015, 107-122.

Jordanova, N., Jordanova, D., Barrón, V., 2019. Wildfire severity: Environmental effects revealed by soil magnetic properties. Land Degradation and Development, 30(18), 2226-2242 .

Kruiver, P., Dekkers M., Heslop, D., 2001. Quantification of magnetic coercivity components by the analysis of acquisition curves of isothermal remanent magnetization. Earth and Planetary Science Letters 189, 269-276.

Kruiver P.P., Langereis C.G., Dekkers M. J. and Krijgsman W., 2003. Rock-magnetic properties of multicomponent natural remanent magnetization in alluvial red beds (NE Spain). Geophys. J. Int., 153, 317–332.

Liu, Q., Roberts, A.P., Torrent, J., Horng Ch-Sh., Larrasoaña, J., C., 2007. What do the HIRM and S- ratio really measure in environmental magnetism? Geochem. Geophys. Geosyst.,8, Q09011, doi:10.1029/2007GC001717.

Long, L.Q., Hue, T.T.B., Hoan, N.X., Cuong, L.V., Thang, P.D., Hoang, T., Truc, T.A., 2016. Growth mechanism and stability of magnetite nanoparticles synthesized by the hydrothermal method. J. Nanosci. Nanotechnol. 16, 7373–7379.

Longworth, G., Becker, L.W., Thompson, R., Oldfield, F., Dearing, J.A., Rummery, T.A., 1979. Mossbauer-effect and magnetic studies of secondary iron-oxides in soils. Journal of Soil Science 30, 93–110.

Lowrie, W., 1990. Identification of ferromagnetic minerals in a rock by coercivity and unblocking temperature properties. Geophysical Research Letters, 17, 159 – 162.

Lu, Sh.-G. Xue, Q.-F., Zhu, L., Yu, J.-Y., 2008. Mineral magnetic properties of a weathering sequence of soils derived from basalt in Eastern China. Catena, 73, 23-33.

Maher, B., 1986. Characterization of soils by mineral magnetic measurements. Phys. Earth Planet. Inter. 42, 76–92.

Maher, B., 1988. Magnetic properties of some synthetic sub-micron magnetites. Geophys. J. R. Astr. Soc., 94, 83-96.

Maher, B., and Taylor, R., 1988. Formation of ultra fine-grained magnetite in soils. Nature, 336, 368-370.

Marchev, P., Singer, B., Jelev, D., Hasson, S., Moritz, R., Bonev, N. , 2004. The Ada Tepe deposit: a sediment-hosted, detachment fault-controlled, low sulfidation gold deposit in the Eastern Rhodopes, SE Bulgaria. Schweiz. Mineral. und Petrogr. Mitt. 84: 59-78

Marinova, I., 2006. Replacement textures from the electrum-bearing, layer-like pervasive silicification in the low sulfidation Khan Krum gold deposit, SE Bulgaria. Compt. rend. Acad. bulg. Sci., 59, 9, 945-948

821 Marinova, I., Ganev, V., Titorenkova, R., 2014. Colloidal origin of colloform-banded textures
822 in the Paleogene low-sulfidation Khan Krum gold deposit, SE Bulgaria. Miner
823 Deposita, 49; 49–74.
824 Maxbauer, D.P., Feinberg, J.M., & Fox, D.L., 2016. MAX UnMix: A web application for
825 unmixing magnetic coercivity distributions. Computers & Geosciences, 95, 140-145.
826 Murad, E., Wagner, U., 1998. Clays and clay minerals: the firing process. Hyperfine Interact.
827 117, 337–356.
828 O`Brien, W., 1994. Mount Gabriel. Bronze Age Mining in Ireland. Galway University Press;
829 First Edition Edition, 371pp
830 Özdemir O. and Dunlop, D., 2000. Intermediate magnetite formation during dehydration of
831 goethite, Earth and Planetary Science Letters 177, 59–67
832 Popov H. and Jockenhövel A., 2011. At the northern borders of the Mycenean world:
833 Thracian gold mining from the Late Bronze and the Early Iron Age at Ada Tepe in the
834 eastern Rhodopes, Anodus: Studies of the Ancient World 10/2010, 265–281.
835 Popov, H, Tsintsov, Z., Jockenhövel, A., Georgiev, P., 2014. Feuersetzen beim Abbau der
836 goldhaltigen Quarzgängen im spätbronzezeitlichen Goldbergwerk auf dem Ada Tepe,
837 Südbulgarien. Experimentelle Archäologie in Europa. Bilanz 2014, Heft 13, 27-44.
838 Popov, H., Koleva, M., Andonova A., Dimitrova, J., Vălčev, I., 2017. Das Goldbergwerk auf
839 dem Ada Tepe. Zu Topografie, Stratigrafie, Chronologie und Interpretation des
840 Nordareals. Archaeologia Austriaca, Band 101/2017, 161–204.
841 Popov H. and Jockenhövel A., 2018. The Late Bronze Age Gold Mine at Ada Tepe. In: Golf
842 & Bronze: Metals, Technologies and Interregional Contacts in the Eastern Balkans
843 during the Bronze Age. Eds: Alexandrov, S., Dimitrova, Y., Popov, H., Horejs, B.,
844 Chukalev, K. National Archaeological Institute with Museum, Bulgarian Academy of
845 Sciences, 590pp. ISBN: 978-954-9472-60-8; 193-205.
846 Popov, H., 2018. Ada Tepe near Krumovgrad, Eastern Rhodope Mountain. In: S. Alexandrov,
847 Y. Dimitrova, H. Popov, B. Horejs, K. Chukalev (eds.), Gold and Bronze. Metals,
848 Technologies and Interregional Contacts in the Eastern Balkans during the Bronze
849 Age, Sofia, 402-415.
850 Popov, H. and Nikov, K. 2018. Ada tepe Lare Bronze Age Gold Mine. Project:Between
851 Borders. In: S. Gimatzidis, M. Pienazek, S. Mangaloğlu-Vortuba (eds.). Archaeologu
852 Across Frontiers and Borderlands. Fragmentation and Connectivity in the North
853 Aegean and the Central Balkans from the Bronze Age to the Iron Age. (= Oriental and
854 European Archaeology, Volume 9). Vienna, 359-389.

Robertson, D.J. and France, D.E., 1994. Discrimination of remanence-carrying minerals in mixtures, using isothermal remanent magnetisation acquisition curves, Phys. Earth planet. Inter., 84, 223–234.

Stöllner, T., 2012. Feuersetzen im frühesten Metallerzbergbau und ein Experiment im frühbronzezeitlichen Goldbergbau von Sakdrissi, Georgien. In: K. Oegl, V. Schaffer (Hrsg.). Die Geschichte des Bergbaus in Tirol und seinen angrenzenden Gebieten. Proceedings zum 6. Milestone-Meeting des SFB HiMAT vom 3.-5.11.2011 in Klausen, Südtirol, Innsbruck, 65-76.

Taylor, R. and Maher, B., 1987. Magnetite in soils: I. The synthesis of single-domain and superparamagnetic magnetite. Clay Minerals, 22, 411-422.

Tcherkezova, E., Popov, H., Jockenhövel, A. 2014. LiDAR-Daten zur Unterstützung der montanarchäologischen Untersuchungen am spätbronzezeitlichen Goldbergwerk Ada Tepe (Stadt Krumovgrad, Rhodopen/Südostbulgarien). -In. Smolnik, R. [Hrsg.]. ArcheoMontan-2013. Krusna krajina. Erz(gebirgs0landschaft – Ore Landhscape. Arbeits- und Forschungsberichte zur sächsischen Bodenmerkmalpflege. Beiheft 28, Landesamt für Archäologie Dresden 2014, 209-221.

Tsintsov Z., Petrova, N., Mehofer, M., 2016. Ancient Gold Mining at Ada Tepe, East Rhodopes, Bulgaria. Mineralogical Features of Au-Containing Fe-Oxides/Hydroxides from the Ada Tepe Gold Deposit. Their Significance in Clarifying the Ancient Gold Mining. Archaeologia Austriaca, Band 100/2016, 109–117.

Thompson, R. and Oldfield, F., 1986. Environmental Magnetism. Allen&Unwin, London

Torrent, J., Liu, Q.S., Barrón,V., 2010. Magnetic susceptibility changes in relation to pedogenesis in a Xeralf chronosequence in northwestern Spain. Eur. J. Soil Sci. 61, 161–173.

Vendelboe A.L., Gunnlaugsson H.P., Helgason O., Nørnberg P., 2005. Characterization of burned soil profiles by Moessbauer spectroscopy. Hyperfine Interact., 166, 517–522.

Walden, J., Oldfield, F., Smith, J. (Eds.), 1999. Environmental magnetism. A practical Guide. Technical Guide No 6. Quaternary Research Association, London.

Weisgerber G. and Willies, L., 2000. The use of fire in prehistoric and ancient mining-firesetting. Paléorient, 26, (2), 131-149.

Wells, M., Fitzpatrick, R., Gilkes, R., Dobson, J., 1999. Magnetic properties of metal-substituted haematite. Geophys. J. Int., 138 (2), 571-580.

Zavala, de Celis R., Jordan A., 2014. How wildfires affect soil properties. A brief review. Guadernos de Investigacion Geografica, 40, 2, 311 – 331.

889 Zboril, R., Mashlan M., Petridis D., 2002. Iron(III) Oxides from Thermal Processess
890 Synthesis, Structural and Magnetic Properties, Moessbauer Spectroscopy
891 Characterization, and Applications. Chem. Mater., 14, 969-982.
892
893